Evaluation of a Commercial Surface Vorticity Flow Solver for the Modeling of Propeller-Wing Interaction

Xiaofan Fei*
NASA Langley Research Center, Hampton, VA, 23681, USA

A commercially available surface vorticity flow solver's ability to model propeller-wing interaction effects was evaluated. First, a study was conducted to determine solution sensitivity to simulation parameters. Then, a deflected slipstream experiment was replicated with an actuator disk and wing model. Comparison with experimental data showed that predictions of lift and longitudinal force coefficients matched well at low flap deflections, but experienced offsets in magnitude with increasing flap deflection. Predictions of pitching moment differed significantly from experimental data largely due to the simple actuator disk model being insufficient for capturing the effects of non-zero flow incidence and non-uniform inflow.

I. Nomenclature

C_L = Lift coefficient, includes thrust in lift direction, $\frac{\text{Lift}}{qS}$
C_L'' = Slipstream-normalized lift coefficient, includes thrust in lift direction, $\frac{\text{Lift}}{q''S}$
C_M = Pitching moment coefficient, includes thrust contribution, positive nose-up, $\frac{\text{Pitching moment}}{qS\bar{c}}$
C_M'' = Slipstream-normalized pitching moment coefficient, includes thrust contribution, positive nose-up, $\frac{\text{Pitching moment}}{q''S\bar{c}}$
C_T = Thrust coefficient, $\frac{T}{\rho n^2 D^4}$
C_X = Longitudinal force coefficient, includes thrust in drag direction, negative in drag direction, $\frac{\text{Longitudinal force}}{qS}$
C_X'' = Slipstream-normalized longitudinal force coefficient, includes thrust in drag direction, negative in drag direction, $\frac{\text{Longitudinal force}}{q''S}$
$\bar{c}$ = Mean aerodynamic chord (ft)
D = Propeller diameter (ft)
n = Propeller rotation speed (rev/s)
q = Freestream dynamic pressure, $\frac{1}{2}\rho V^2$ (lb/ft^2)
q'' = Slipstream dynamic pressure, $q + \frac{T}{\frac{\pi}{4}D^2}$ (lb/ft^2)
S = Reference area (ft^2)
T = Propeller thrust (lb)
T_c'' = Slipstream-normalized thrust coefficient, $\frac{T}{q''\frac{\pi}{4}D^2}$
V_∞ = Freestream velocity (ft/s)
ΔV = Velocity increment over freestream of fully developed slipstream (ft/s)
α = Angle of attack (deg)
ρ = Air density (slugs/ft^3)

II. Introduction

The adoption of distributed electric propulsion (DEP) in aviation has led to a renewed interest in the design of propeller-driven aircraft. However, unlike conventional single- or twin- engine aircraft, DEP propeller aircraft are often designed to exploit favorable propeller-airframe interactions for improved aerodynamic performance. It is the presence of and dependence on these interactions that renders traditional propulsion-decoupled conceptual-level aerodynamic analysis tools such as PMARC [1], AVL [2], and XFLR5 [3] ineffective.

The goal of the presented work is to evaluate a new surface vorticity flow solver, FlightStream® [4], in its ability to model propeller-wing interaction. This paper is a compilation of two studies in this area. First, a solution sensitivity

*Pathways Intern, Aeronautics Systems Analysis Branch, 1 N. Dryden St. MS 442, AIAA Student Member.

study was conducted to determine how FlightStream's converged flow solutions in the presence of propeller-wing interaction vary with simulation parameters. Second, FlightStream's actuator disk and wing model is used to replicate a deflected slipstream wind tunnel experiment.

III. FlightStream Overview

Developed by Research In Flight, FlightStream is a surface vorticity flow solver designed to facilitate the conceptual design of aircraft containing complex or unconventional geometries. From the perspective of electric aircraft design, FlightStream is a highly attractive analysis tool because of its quick and simple simulation setup process and its integrated propulsion modeling capabilities. Rapid analyses are enabled by the combination of a robust meshing algorithm, which can quickly produce unstructured isometric surface meshes from imported CAD models, and a versatile scripting interface, which can automate the manipulation of geometries, the addition of propulsion elements, and the setup of solver parameters.

FlightStream produces potential flow solutions by solving for a linearly varying surface vorticity distribution over the unstructured mesh(es). Wakes are modeled by strands of constant vorticity shed from nodes along user-defined trailing edges, where the vorticity strength is calculated as the net flux of vorticity from adjacent edges [5, 6]. Propellers can be modeled in multiple ways in FlightStream. When interaction with another body is desired, propellers can be introduced as a Conway linearized actuator disk [7] with uniform loading [8]. With this simplistic approach, calculated slipstream velocities are superimposed on the flow field in the volume behind the actuator disk. Alternatively, a more detailed analysis of arbitrary propeller geometries in isolation can be performed using the steady-state rotating reference frame mode. In this mode, physical blades are fixed in position while the freestream is prescribed an axial velocity and a rotation speed about the origin. Lastly, an unsteady solver mode is under development which will eventually allow the integration of rotating blades with fixed bodies.

Several efforts have already been made to evaluate FlightStream's various capabilities. King et al. [9] and Ahuja et al. [10] both used FlightStream to optimize engine placement on an airliner in cruise conditions. Olson and Albertson [11] investigated FlightStream's ability to model an airliner with high-lift devices deployed. Sandoz et al. [12] and Johnson et al. [13] both modeled propeller-driven aircraft with the actuator disk approach. Sargent and Anemaat [14] and Anemaat et al. [15] modeled a ducted fan and a rotor, respectively, with the rotating reference frame approach. The overall sentiment seems to be that FlightStream, though not as accurate as higher-order Euler or Navier-Stokes methods, provides an improvement in accuracy over traditional low-order tools at a computational cost acceptable for conceptual design.

The version of FlightStream used in the presented studies is 11.4, build 10232018.

IV. Solution Sensitivity to Simulation Parameters

One of FlightStream's attractive qualities is its potential for rapid design space exploration. Consequently, it is important to understand the trade-offs between computational cost and solution accuracy. A study was conducted to investigate the effects of several computation time-affecting parameters on the converged solution of an actuator disk and wing model. The parameters tested are listed and described in Table 1. A baseline setting was selected, and a univariate sweep was conducted about the baseline for each parameter.

A. FlightStream Model Setup

The geometry used for the sensitivity study was based on the NASA X-57 Maxwell [16] and is shown in Fig. 1. Only the X-57's cruise configuration wing and the high-lift propeller system, consisting of six leading edge propellers on each semispan, were included. The wingtip propeller and nacelles and high-lift propeller nacelles and pylons were omitted for simplicity. The symmetry plane option was enabled to capture the entire span. A single flight condition was specified at V_∞ = 97.9 ft/s and $\alpha = 13°$, and each actuator disk was defined to produce 49.6 lb of thrust at 4547 rpm, rotating inboard-up.

B. Results

The results of the sensitivity study are shown in Figs. 2-5, and for reference, Table 2 gives the solution of the baseline case. In each figure, plot (a) shows the variation in converged C_L, C_X, and C_M values after being normalized by the respective metric value of the baseline case. Plot (b) shows the variation in simulation time, also normalized by

Table 1 List of simulation parameters varied. Bold values denote the baseline setting.

Parameter Name	Settings	Units	Description
Mesh refinement	1300, 2800, **6100**, 11700, 23500, 47300	Faces	Number of faces comprising an unstructured isotropic mesh generated with FlightStream's trimmed mesher.
Convergence limit	0.0004, 0.0002, **0.0001**, 0.00005		Value that residuals of lift, drag, and pitching moment coefficients must be less than for the solution to be considered converged.
Wake size	800, 400, 200, **100**, 50, 25	%	Length of wake strand segments as a percentage of the average mesh edge length. Smaller values result in more wake segments per unit length.
Trefftz plane distance	2, 4, **8**, 16, 32	$\bar{c}$	How far downstream wake strands extend relative to wing trailing edge, as a multiple of the mean aerodynamic chord.

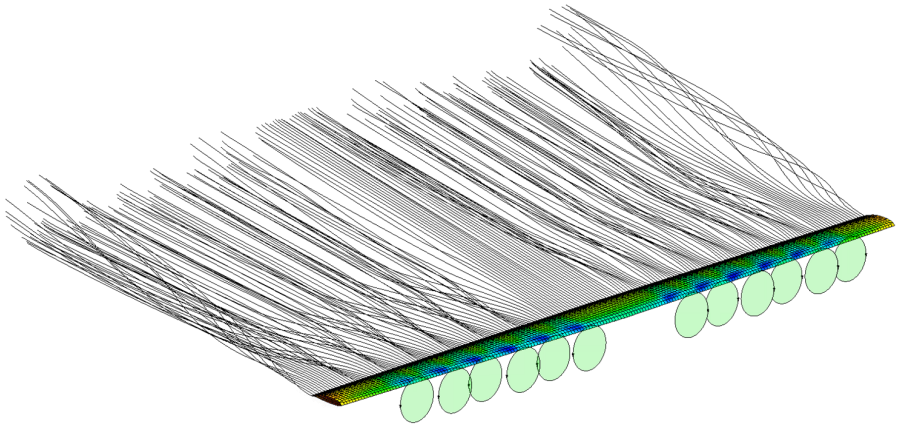

Fig. 1 X-57 wing and high-lift propeller system modeled in FlightStream with baseline settings defined in Table 1.

the simulation time required for the baseline case. Note that the inverse of the parameter setting value was used as the x-axis for wake size (Fig. 4) and convergence limit (Fig. 5) because the setting values of these two parameters decrease with increasing modeling fidelity.

Table 2 Solution metrics of the sensitivity study baseline case.

C_L	C_X	C_M	Simulation time (s)
3.125	-0.4905	-0.0912	18.55

Mesh refinement was found to have the largest effect on converged solution metrics. Figure 2(a) shows that pitching moment is especially sensitive to mesh refinement, asymptoting to a value 22% higher than that of the baseline's pitching moment as the mesh face count increases. Lift and longitudinal force coefficients are less sensitive, but can still err by several percent with insufficient mesh refinement. Unfortunately, mesh refinement is also the most computationally expensive to increase. Quadrupling the face count corresponds to a 15 fold increase in simulation time because the finer mesh also increases the number of wake strands spawned from the trailing edge.

Inspection of Figs. 3 and 4 reveals that, in terms of wake modeling fidelity, computational effort is better spent on increasing wake length via a larger Trefftz plane distance than on increasing the number of wake segments per unit length via a smaller wake size. The effect of Trefftz plane distance, which leads to variations of a few percent in the converged solution metrics, is an order of magnitude greater than that of wake size while also costing less simulation

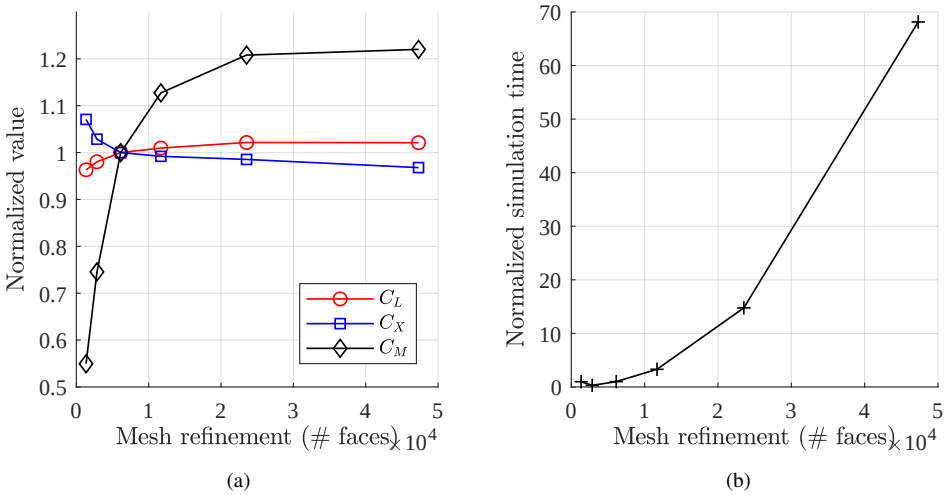

(a) (b)

Fig. 2 Variation of converged solution metrics and computation time with mesh refinement.

time to increase. However, this trade-off may not be valid if the wing wake is expected to interact with other bodies as increasing wake size increases the coarseness of the wake discretization, thereby reducing the ability of the wake strands to deform. Lastly, convergence limit (Fig. 5) was found to have the least impact on both converged solution metrics and computation time. This parameter can be safely relaxed, at least in the range of values tested.

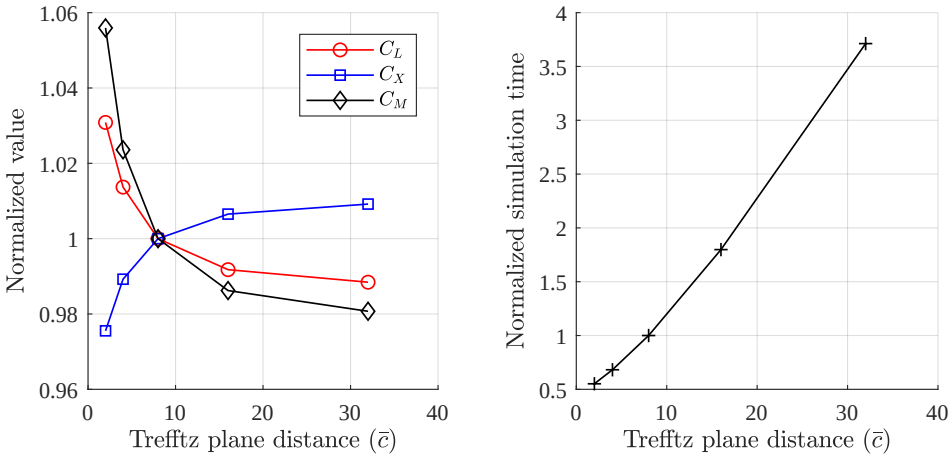

(a) (b)

Fig. 3 Variation of converged solution metrics and computation time with Trefftz plane distance.

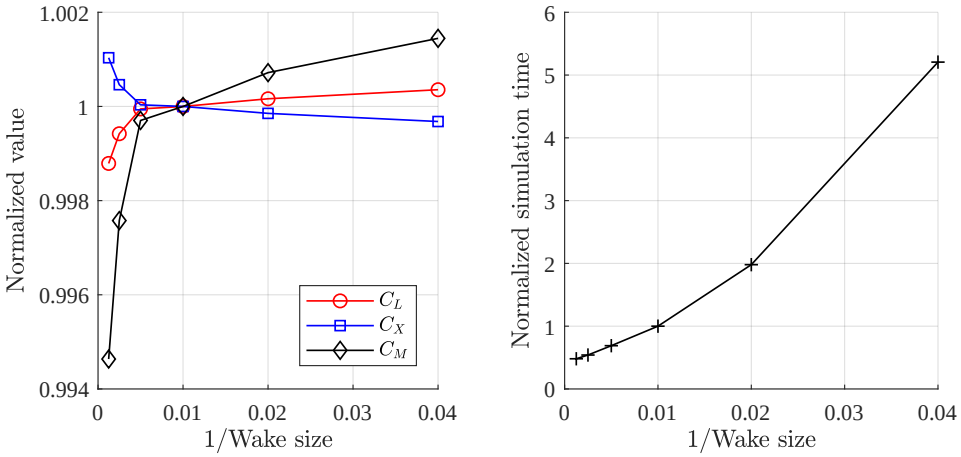

Fig. 4 Variation of converged solution metrics and computation time with wake size.

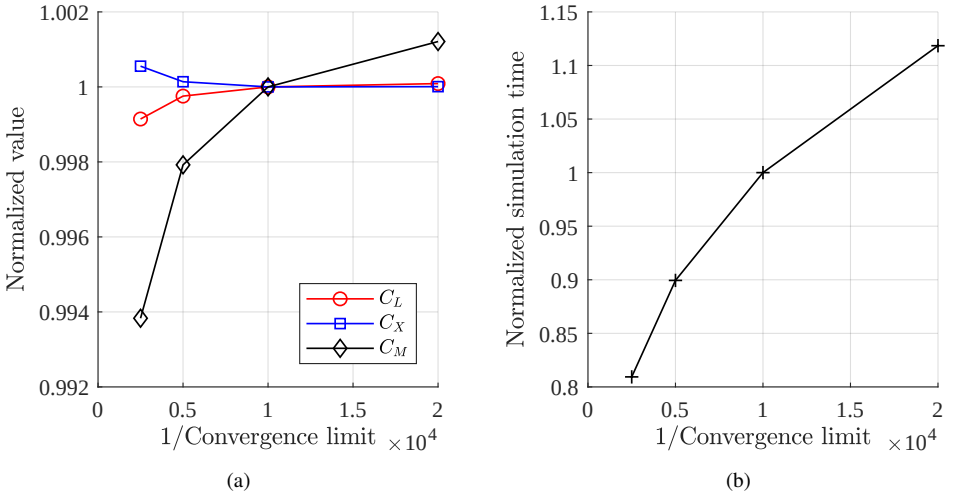

Fig. 5 Variation of converged solution metrics and computation time with convergence limit.

V. Actuator Disk and Wing Model of a Wind Tunnel Experiment

A. Experiment Overview

A deflected slipstream wind tunnel experiment by Kuhn and Draper [17] was selected to test FlightStream's actuator disk approach for modeling propeller-wing interaction. This experiment involved a 3.416 ft semispan wing with a double plain flap, hinged at 30% and 60% chord as measured from the trailing edge. The semispan wing was blown by a pair of 2 ft diameter propellers and was designed to investigate the effectiveness of a flapped wing at deflecting propeller slipstreams for vertical takeoff. The experimental setup is depicted in Fig. 6.

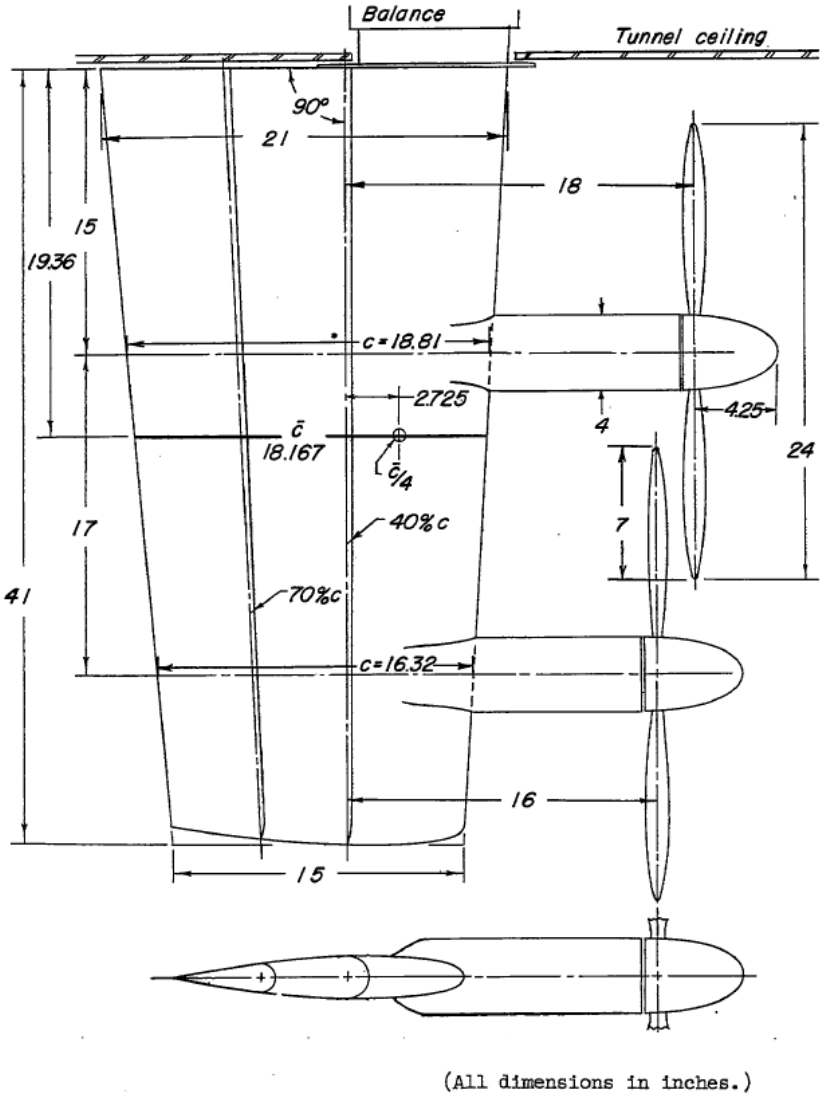

Fig. 6 Kuhn and Draper's wind tunnel model, taken from Fig. 2 of Ref. [17].

Since their experiment included static conditions, Kuhn and Draper normalized forces and moments by the slipstream dynamic pressure, q'', instead of freestream dynamic pressure. The resulting coefficients, denoted by the double prime notation (e.g. C_L''), would not tend toward infinity as freestream velocity neared zero. Similarly, a slipstream-normalized thrust coefficient, T_c'', was used to quantify the propeller's contribution to the slipstream dynamic pressure. T_c'' has the convenient behavior of equaling 0 when there is no propeller thrust and equaling 1 when there is no freestream velocity (i.e. static thrust only).

The experiment was designed such that the slipstream dynamic pressure would remain constant for all test conditions.

At each freestream condition, the rotation speed of the inboard propeller was adjusted to achieve the thrust required to maintain $q'' = 8$ lb/ft^2 at $\alpha = 0°$. The outboard propeller, which nominally operated at the same rotation speed as the inboard propeller, was trimmed in collective pitch to match thrusts with the inboard propeller. The thrust target for $\alpha = 0°$ was also applied for tests at non-zero angles of attack and was achieved by the same means. This experimental design meant that each freestream condition corresponded to a unique T_c'' and thrust loading condition, four of which were selected for this study. Kuhn and Draper also tested a wide range of flap deflection combinations. Only three flap configurations representative of commonly used flap settings on small aircraft were selected for this study. A summary of the subset of test conditions replicated in FlightStream is given in Table 3, while a comprehensive description of Kuhn and Draper's experiment can be found in Ref. [17].

Table 3 Summary of experimental cases from Ref. [17] replicated in FlightStream.

T_c''	T (lb, per prop)	q (lb/ft^2)	V_∞ (ft/s)	q'' (lb/ft^2)	$V_\infty + \Delta V$ (ft/s)
0	0	8.00	82.0	8	82
0.50	12.5	4.00	57.9	8	82
0.71	17.6	2.32	44.2	8	82
0.91	22.6	0.72	24.6	8	82

Flap deflection, 30% flap (deg)	0, 10, 30
Flap deflection, 60% flap (deg)	0
Angle of attack (deg)	approximately -10° to 30°
All cases have both propellers operating.	

B. FlightStream Model Setup

A CAD model of the semispan wing and nacelles was imported into FlightStream where an unstructured isotropic geometry mesh was generated with about 26,000 faces* and 105 wake strand nodes at the trailing edge. The relaxed wake setting was used with a 1200% wake size and with the Trefftz plane set at a distance of 32 times the mean aerodynamic chord. The symmetry plane option was turned on to mimic the presence of the wind tunnel wall as a reflection plane, and a turbulent boundary layer model was selected to estimate viscous drag. An example of the resulting geometry is shown in Fig. 7. Convergence of the flow solution was determined by a limit on residuals; lift, drag, and pitching moment coefficients were required to change by no more than 0.0005 between iterations for a solution to be considered converged.

FlightStream's propeller actuator disk model is defined by a rotation speed and thrust coefficient (C_T). Unfortunately, while the propeller thrusts were trimmed to known values, Ref. [17] did not document the propellers' rotation speeds or the atmospheric conditions during the experiment. Instead, the propeller rotation speeds were estimated by using data from an earlier experiment by Draper and Kuhn [18]† that tested the same wing and propeller. Ref. [18] provides measurements of effective advance ratio ($V_\infty \cos(\alpha)/nD$) vs. α at the same T_c'' settings seen in Ref. [17], albeit only in the presence of the wing with flaps retracted. By assuming an air density of $\rho = 0.002328$ slugs/ft^3 and that the target thrusts at each T_c'' were achieved at the effective advance ratios documented in [18], an estimate of n could be solved for and used to calculate the C_T that would have been observed during the experiment in Ref. [17]. This approach is limited in that propeller rotation speeds could not vary with flap deflection due to the lack of data.

C. Results

Appendix A contains the compilation of experimental data versus FlightStream prediction plots for the cases summarized in Table 3. Figs. 8-10, 11-13, and 14-16 are grouped by flap deflections (of the 30% flap) of 0°, 10°, and 30°, respectively. Each figure is dedicated to one of three metrics, C_L'', C_X'', or C_M'', while the subplots within each figure are differentiated by T_c''. It should be noted that the metrics of C_L'', C_X'', and C_M'' include contributions from the propeller.

*The face counts given here are those of the geometric meshes. FlightStream's solver then applies a quad mesh filter that combines pairs of adjacent triangular faces into quadrilaterals in well-behaved regions, reducing the final face counts by about half.

†An updated version of this publication with clearer graphs is found in Ref. [19].

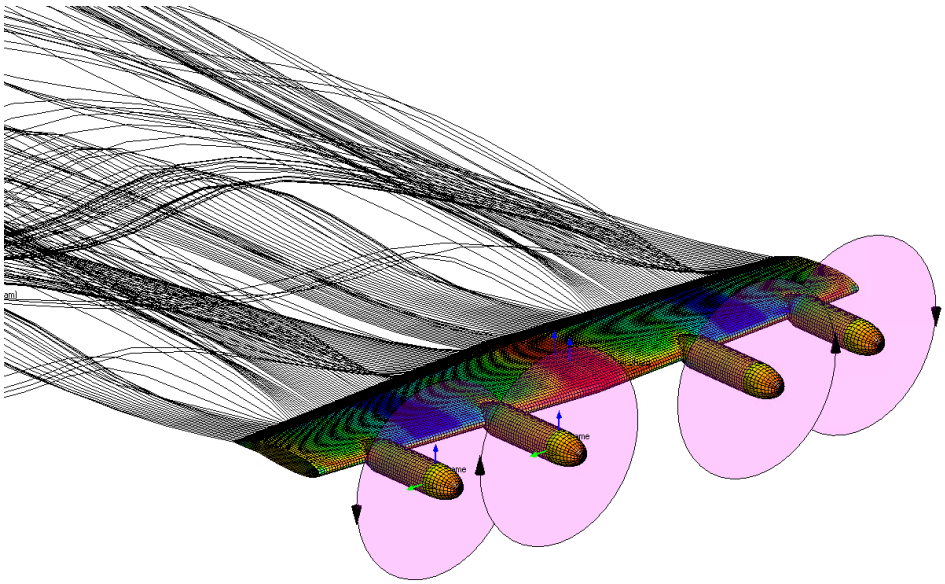

Fig. 7 Kuhn and Draper's wind tunnel experiment modeled in FlightStream. The configuration shown is with the 30% flap deflected at 10°.

FlightStream was found to predict C_L'' with good accuracy for cases with 0° flap deflection (Fig. 8). The inability of potential flow methods to capture stall are clearly seen in the unblown case (Fig. 8(a)), but FlightStream's predictions for blown cases are valid for a much wider range of angle of attack due to the delay in stall. As flap deflection increases (Figs. 11 and 14), FlightStream increasingly overpredicts C_L'' values, although the slopes ($dC_L''/d\alpha$) still match well. This offset is, again, likely a limitation of the potential flow method in not capturing flow separation effects.

Aside from post-stall discrepancies, predictions of C_X'' match well for flap deflections of 0° and 10° (Figs. 9 and 12). However, at 30° flap deflection, FlightStream's predictions of C_X'' differ significantly from experimental data. The nearly constant underprediction in drag observed in the unblown case (Fig. 15(a)) is likely another symptom of not capturing drag additional due to flow separation effects, but the differences in slope seen in the blown cases (Fig. 15(b), 15(c), and 15(d)) indicate a separate issue. A possible explanation is an incorrect estimation of the n and C_T used to define FlightStream's actuator disks. The approach of using data from Ref. [18] produced n and C_T values based off of the propellers' performance in the presence of a wing with zero flap deflection. Therefore, it is understandable that errors should arise as the flap deflection increases.

Predictions of C_M'' only match well for the unblown case with 0° flap deflection before stall (Fig. 10(a)). As flap deflection increases, C_M'' for unblown cases (Figs. 13(a) and 16(a)) maintain a reasonable match in slope ($dC_M''/d\alpha$) in the unstalled region but become increasingly overpredicted in magnitude. When blowing is applied, C_M'' is seen to differ significantly from experimental results, regardless of the flap deflection ((b), (c), and (d) of Figs. 10, 13, and 16). Judging by the consistently shallower slopes, it is hypothesized that the cause of error is the lack of normal force and pitching moment on the actuator disks themselves. Kuhn and Draper [17] observed that the propellers experienced large normal forces and positive pitching moments at high angles of attack due to wing upwash and non-uniform inflow, respectively. FlightStream's actuator disks only produce a thrust force normal to the disk and are, therefore, unable to capture these additional effects.

Fortunately, Kuhn and Draper provided measurements of propeller normal force and pitching moment observed during their experiment (Figs. 29 and 30 of Ref. [17]), and an initial effort was made to correct FlightStream's predictions by adding the experimentally measured propeller contributions to pitching moment. Kuhn and Draper mentioned that the measurements for the inboard propeller experienced excessive scatter due to problems with the force sensor, so measurements for the outboard propeller were doubled as an approximation. After adjusting for reference area, the experimental propeller pitching moment coefficients and the experimental propeller normal force coefficients multiplied by the propellers' moment arms were added to FlightStream's pitching moment prediction. The corrected predictions are denoted in Figs. 10, 13, and 16 as "FS+cor." Despite the impreciseness of the correction, the resulting curves match experimental data reasonably well and are a considerable improvement over the uncorrected predictions.

VI. Conclusion

The presented work evaluated a commercial surface vorticity flow solver, FlightStream, in its ability to model propeller-wing interaction effects with an actuator disk and wing model. A sensitivity study was first conducted to determine appropriate settings for simulation parameters. Mesh refinement was found to have the largest effect, requiring over 20,000 faces before the converged solution metrics became insensitive to further refinement. Trefftz plane distance had the second largest effect, leading to variations of a few percent in the converged solution metrics, but the computation expense associated with increasing the Trefftz plane distance could be offset by increasing the wake size with little penalty to solution accuracy.

A wind tunnel experiment involving a blown wing with plain flaps was then replicated in FlightStream. Comparisons with experimental data showed that lift and longitudinal force can be predicted well for low flap deflections. Higher flap deflections induced an offset from experimental data, which is suspected to be a result of the presence of flow separation effects not captured in FlightStream. Pitching moment predictions were initially poor for blown cases but were greatly improved when experimentally measured propeller normal force and propeller pitching moment contributions were added. The results suggest that two types of modifications are required before FlightStream can be used to accurately model propeller-wing interaction. First, a correction is required to account for flow separation effects resulting from flap deflections. Second, a more sophisticated propeller model is required in order to capture propeller normal forces and propeller pitching moments resulting from non-zero flow incidence and non-uniform inflow conditions, respectively.

A. Appendix

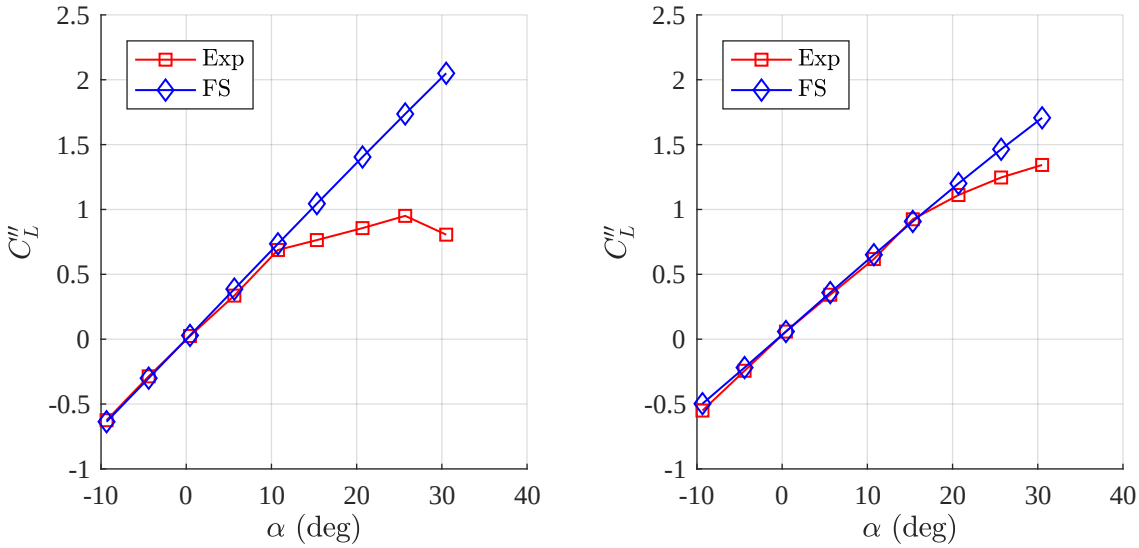

(a) $T_c'' = 0$ (b) $T_c'' = 0.50$

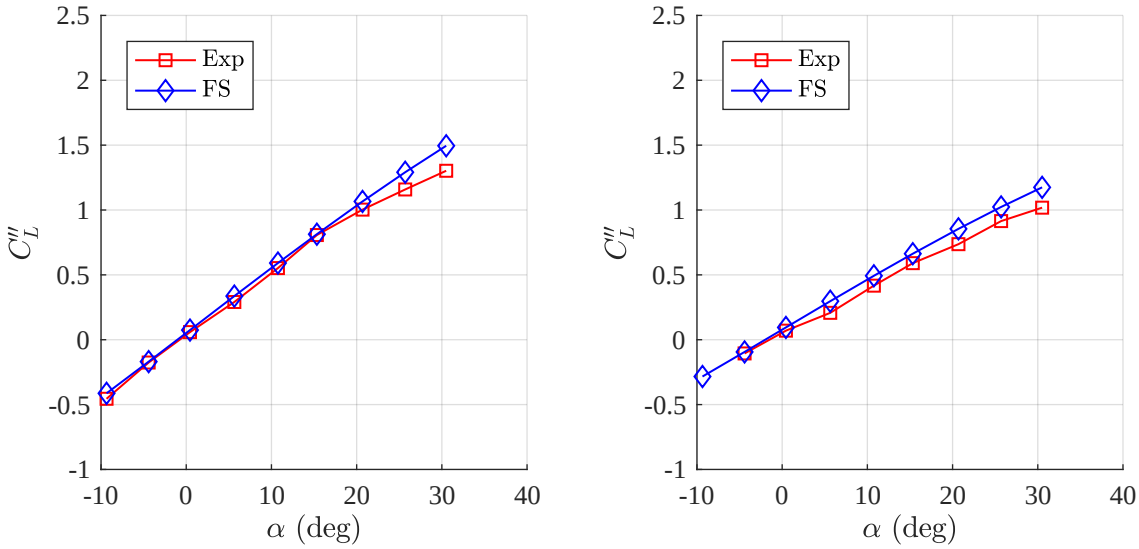

(c) $T_c'' = 0.71$ (d) $T_c'' = 0.91$

Fig. 8 Comparison of experimental data and FlightStream predictions of slipstream-normalized lift coefficient vs. angle of attack for varying slipstream-normalized thrust coefficients. 30% flap deflected 0°.

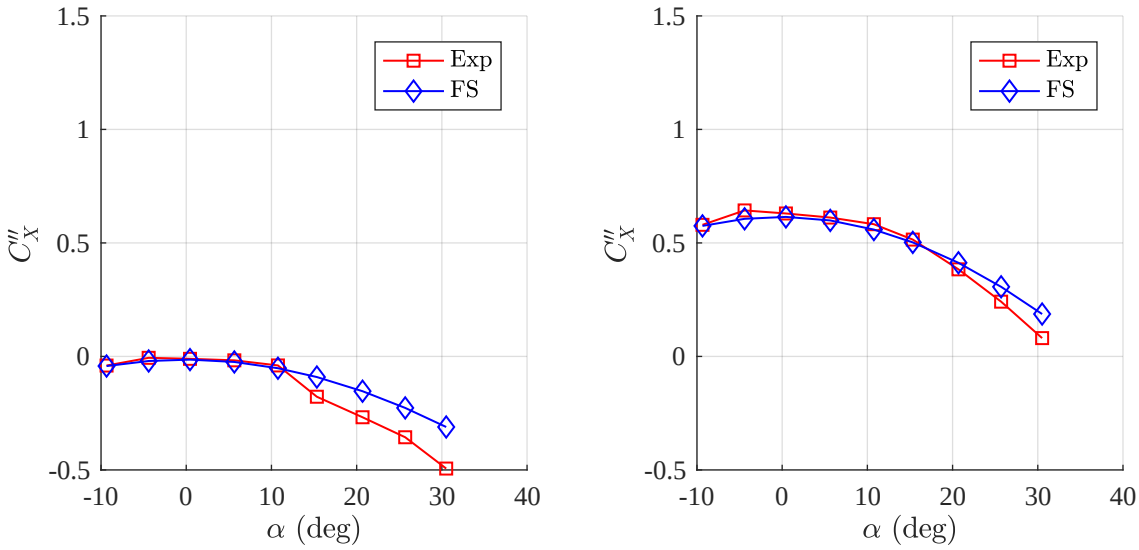

(a) $T''_c = 0$ (b) $T''_c = 0.50$

(c) $T''_c = 0.71$ (d) $T''_c = 0.91$

Fig. 9 Comparison of experimental data and FlightStream predictions of slipstream-normalized longitudinal force coefficient vs. angle of attack for varying slipstream-normalized thrust coefficients. 30% flap deflected 0°.

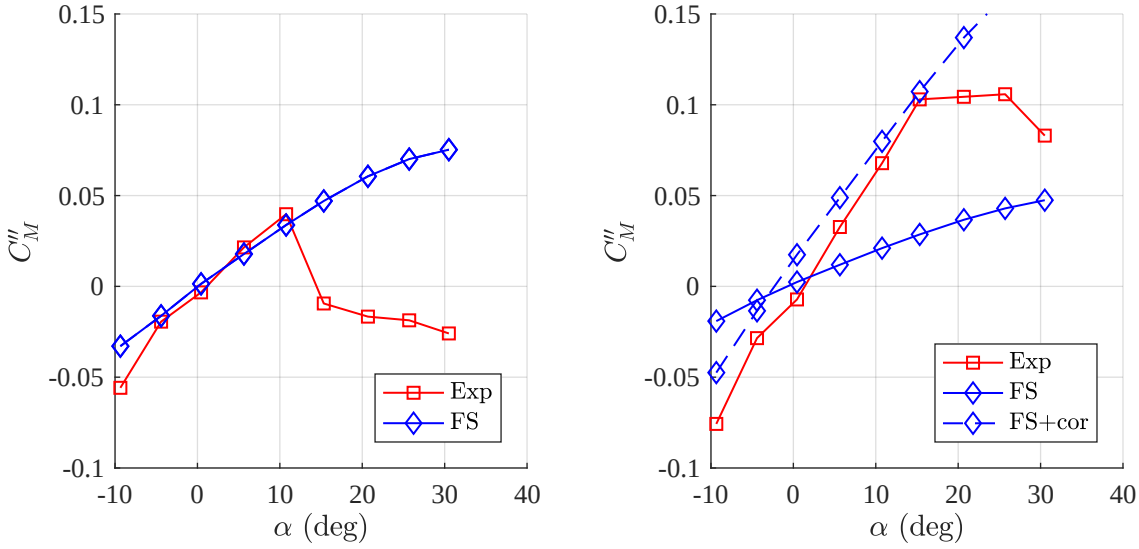

(a) $T''_c = 0$

(b) $T''_c = 0.50$

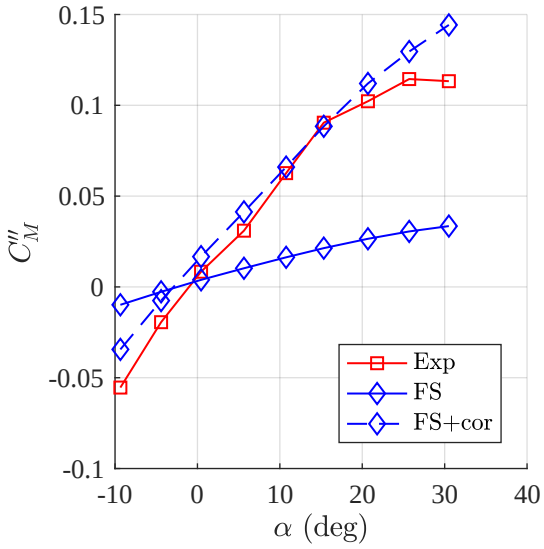

(c) $T''_c = 0.71$

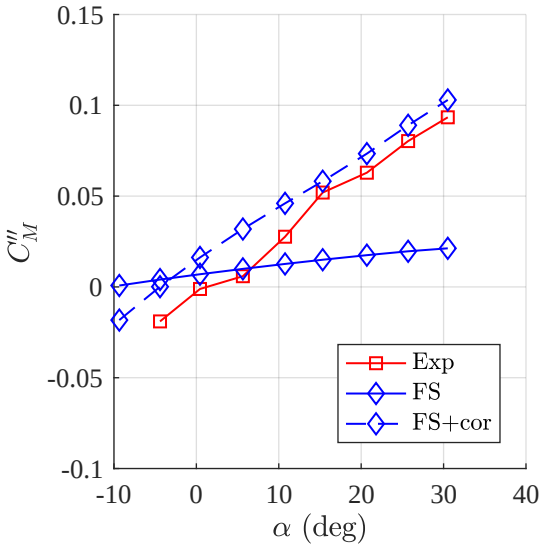

(d) $T''_c = 0.91$

Fig. 10 Comparison of experimental data and FlightStream predictions of slipstream-normalized pitching moment coefficient vs. angle of attack for varying slipstream-normalized thrust coefficients. 30% flap deflected 0°.

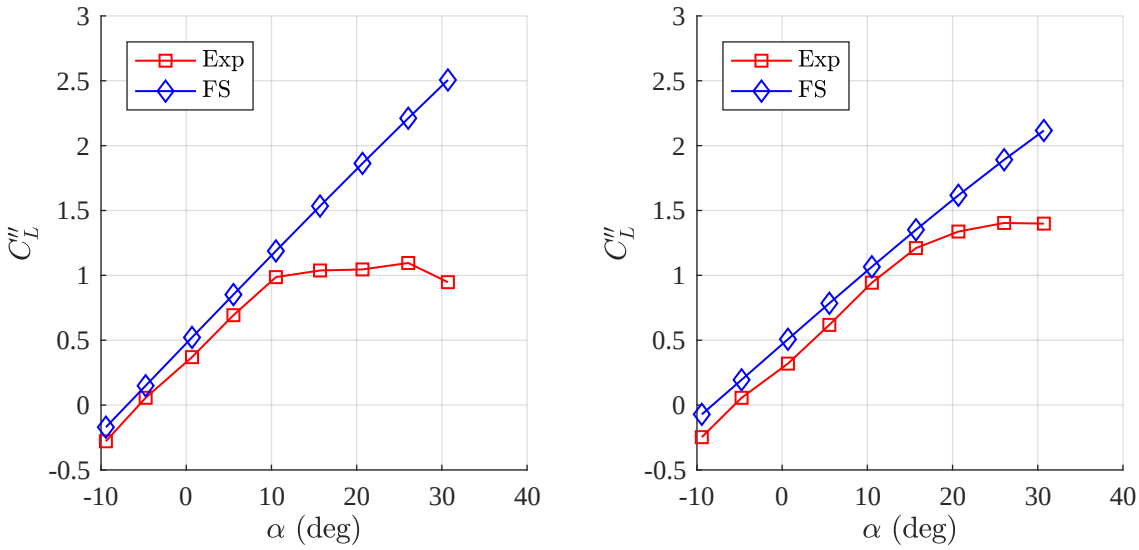

(a) $T_c'' = 0$ (b) $T_c'' = 0.50$

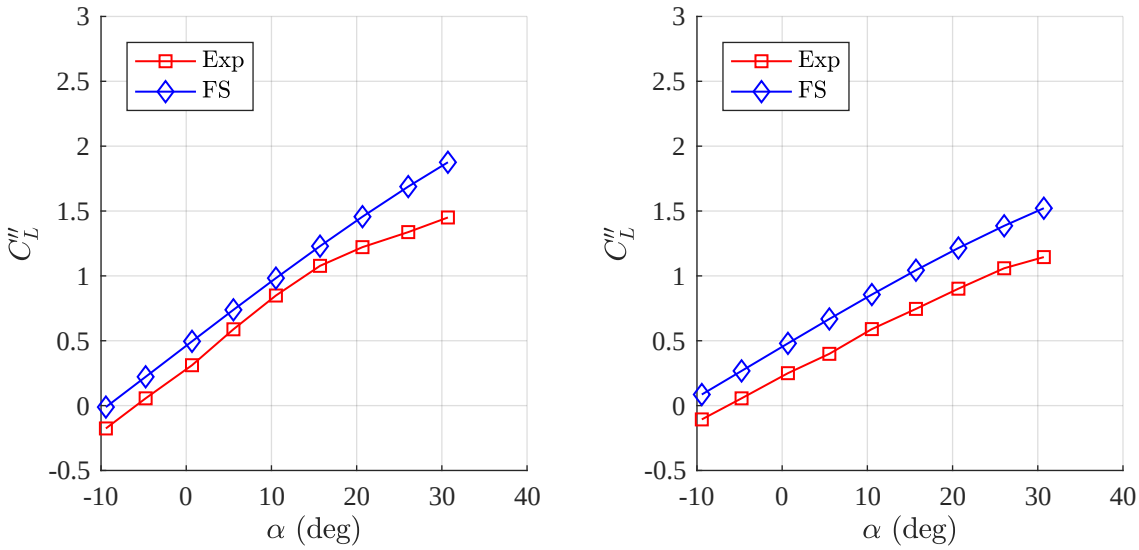

(c) $T_c'' = 0.71$ (d) $T_c'' = 0.91$

Fig. 11 Comparison of experimental data and FlightStream predictions of slipstream-normalized lift coefficient vs. angle of attack for varying slipstream-normalized thrust coefficients. 30% flap deflected 10°.

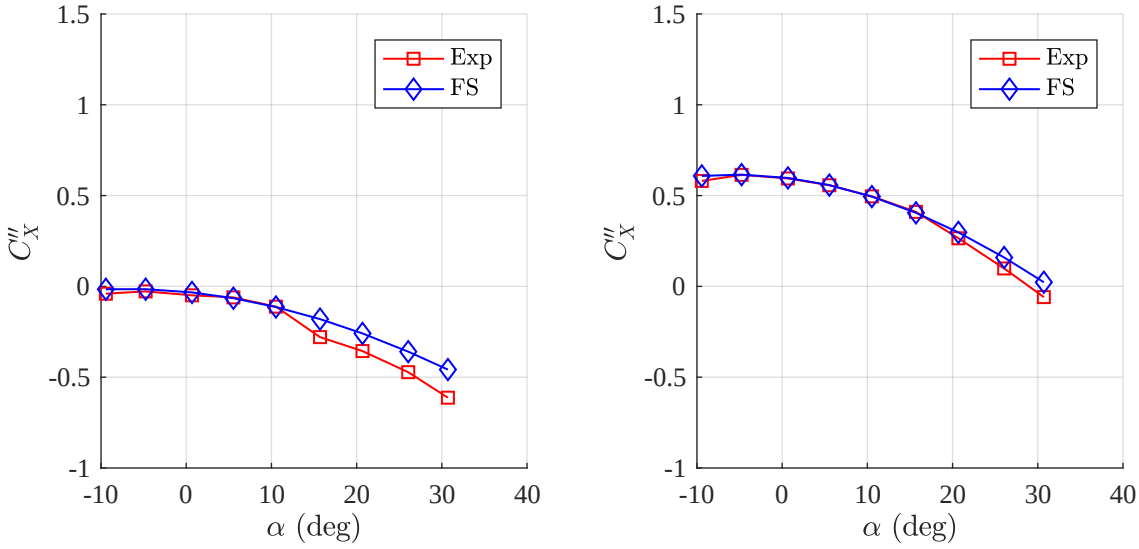

(a) $T_c'' = 0$ (b) $T_c'' = 0.50$

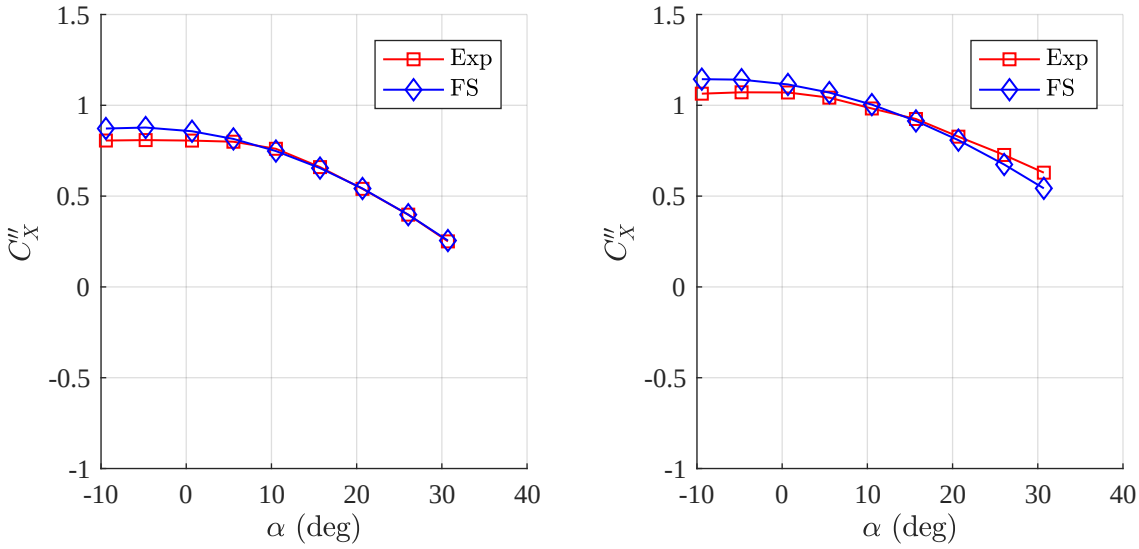

(c) $T_c'' = 0.71$ (d) $T_c'' = 0.91$

Fig. 12 Comparison of experimental data and FlightStream predictions of slipstream-normalized longitudinal force coefficient vs. angle of attack for varying slipstream-normalized thrust coefficients. 30% flap deflected 10°.

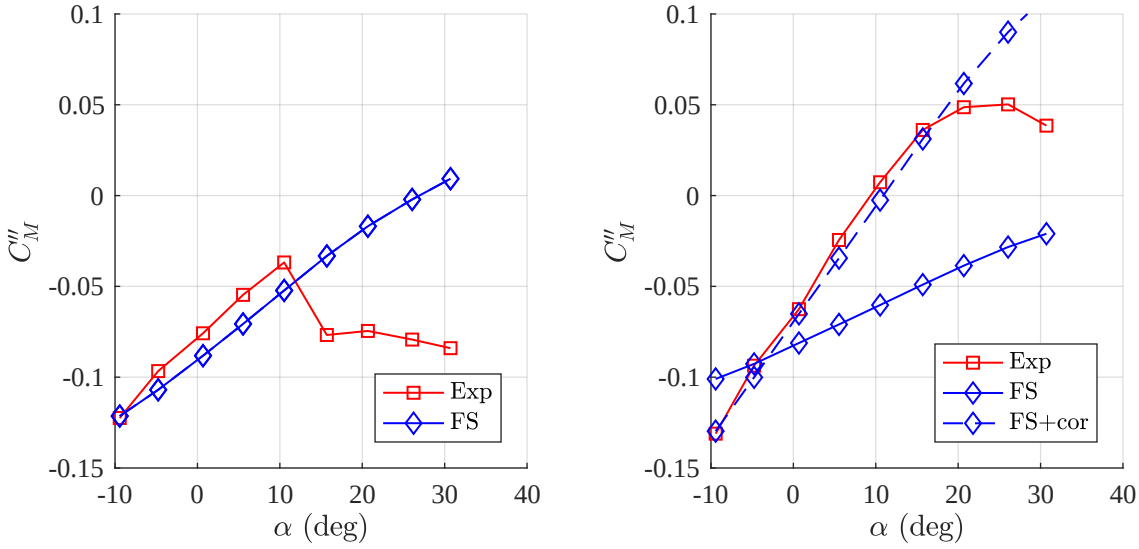

(a) $T''_c = 0$

(b) $T''_c = 0.50$

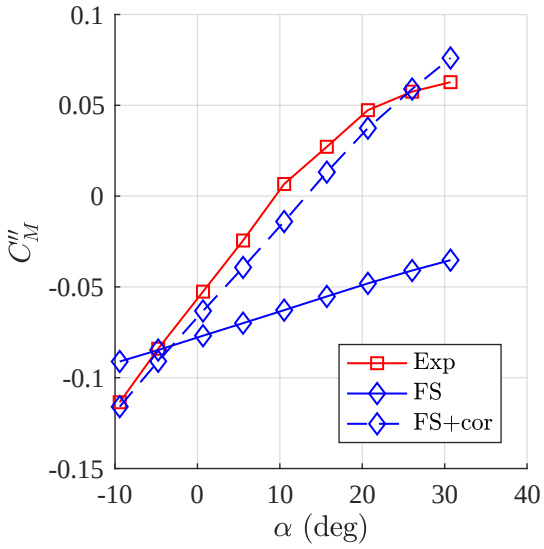

(c) $T''_c = 0.71$

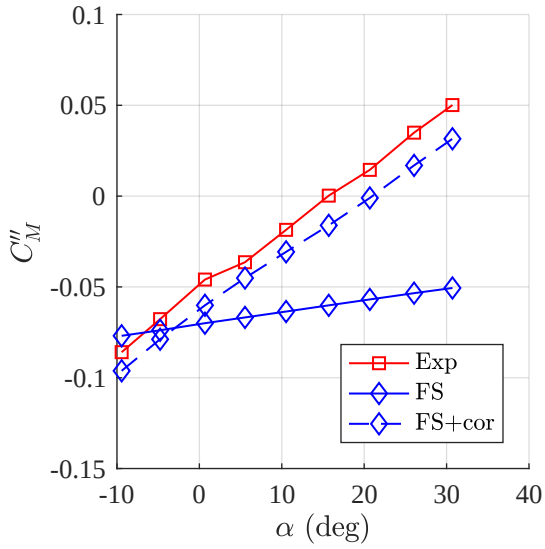

(d) $T''_c = 0.91$

Fig. 13 Comparison of experimental data and FlightStream predictions of slipstream-normalized pitching moment coefficient vs. angle of attack for varying slipstream-normalized thrust coefficients. 30% flap deflected 10°.

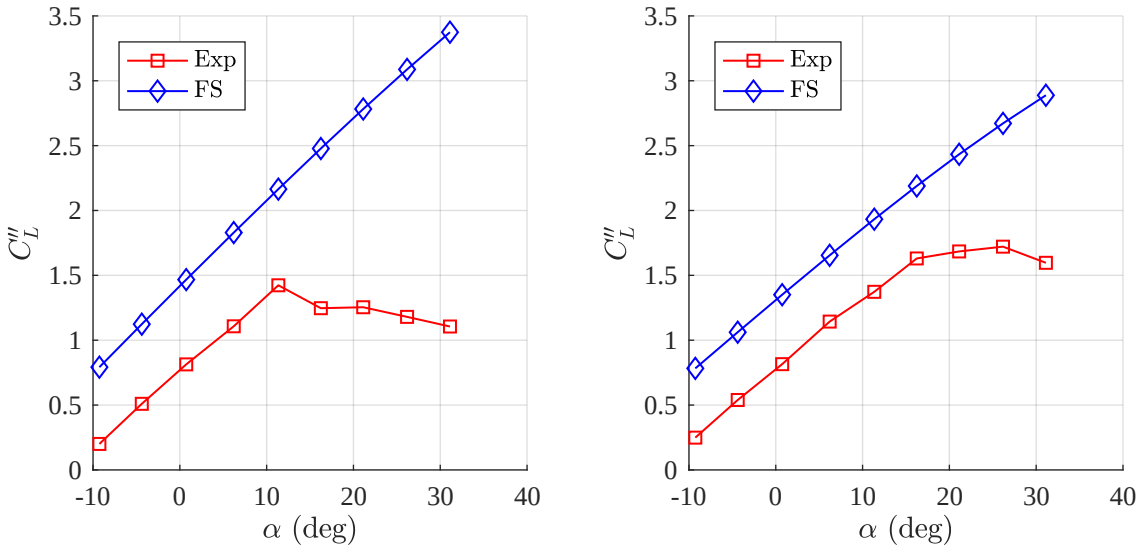

(a) $T_c'' = 0$ (b) $T_c'' = 0.50$

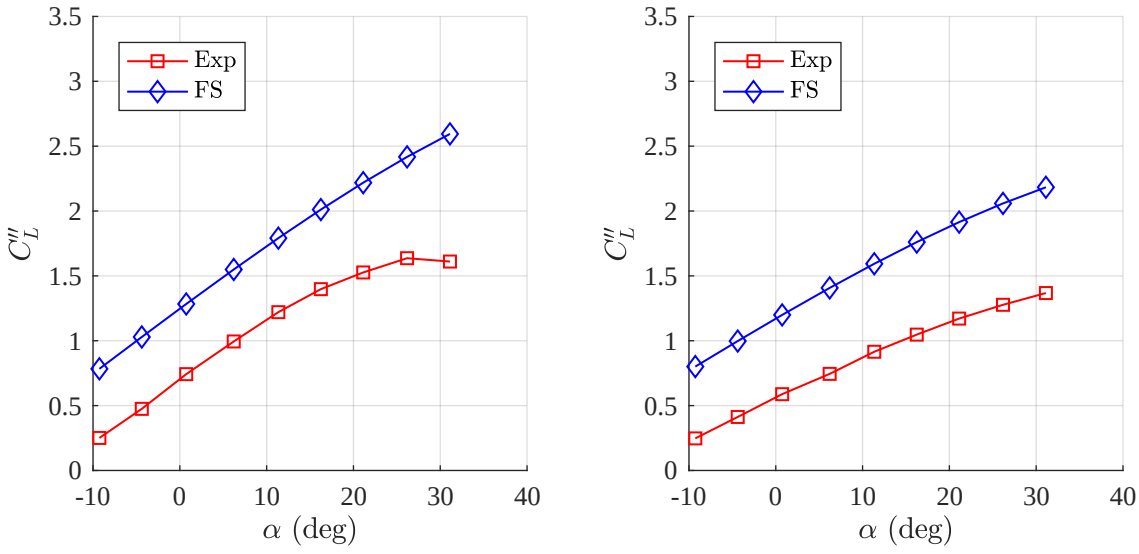

(c) $T_c'' = 0.71$ (d) $T_c'' = 0.91$

Fig. 14 Comparison of experimental data and FlightStream predictions of slipstream-normalized lift coefficient vs. angle of attack for varying slipstream-normalized thrust coefficients. 30% flap deflected 30°.

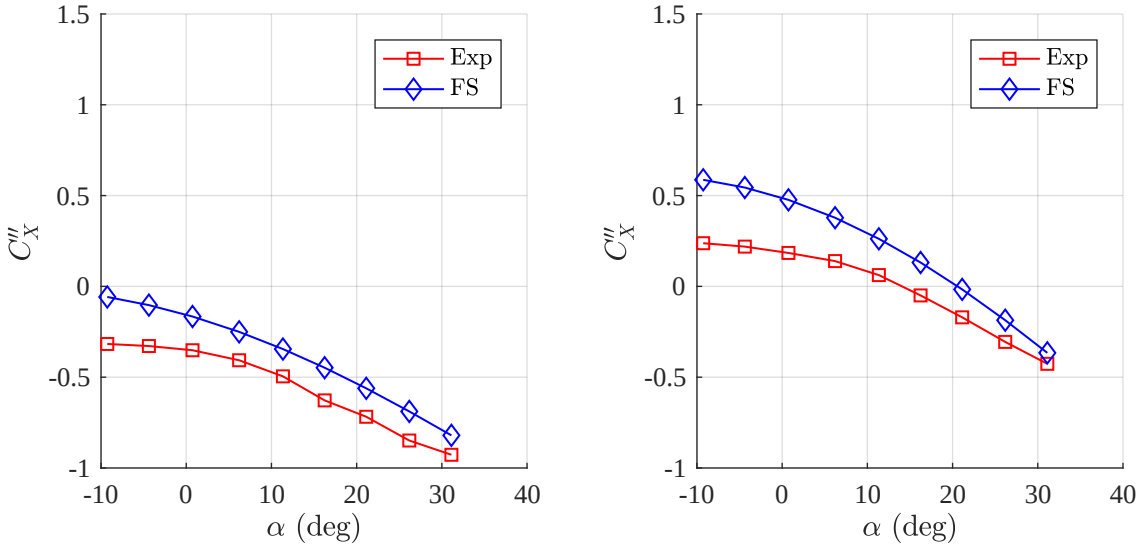

(a) $T''_c = 0$

(b) $T''_c = 0.50$

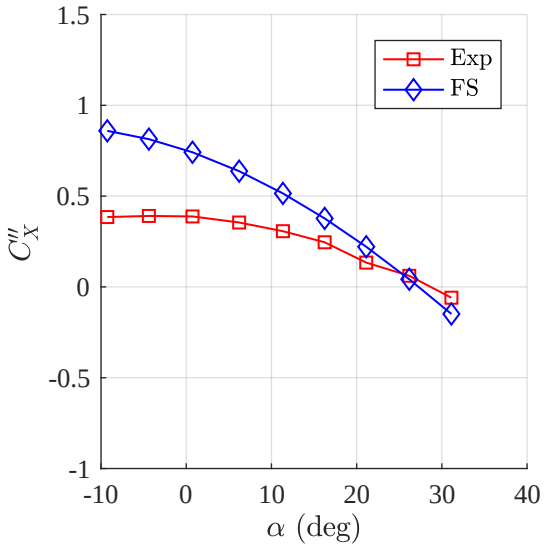

(c) $T''_c = 0.71$

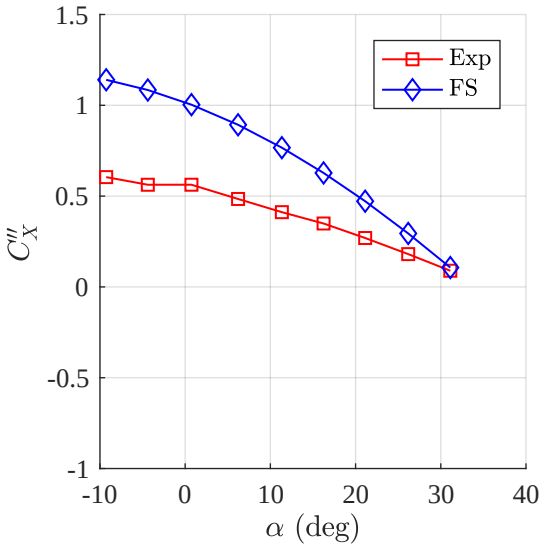

(d) $T''_c = 0.91$

Fig. 15 Comparison of experimental data and FlightStream predictions of slipstream-normalized longitudinal force coefficient vs. angle of attack for varying slipstream-normalized thrust coefficients. 30% flap deflected 30°.

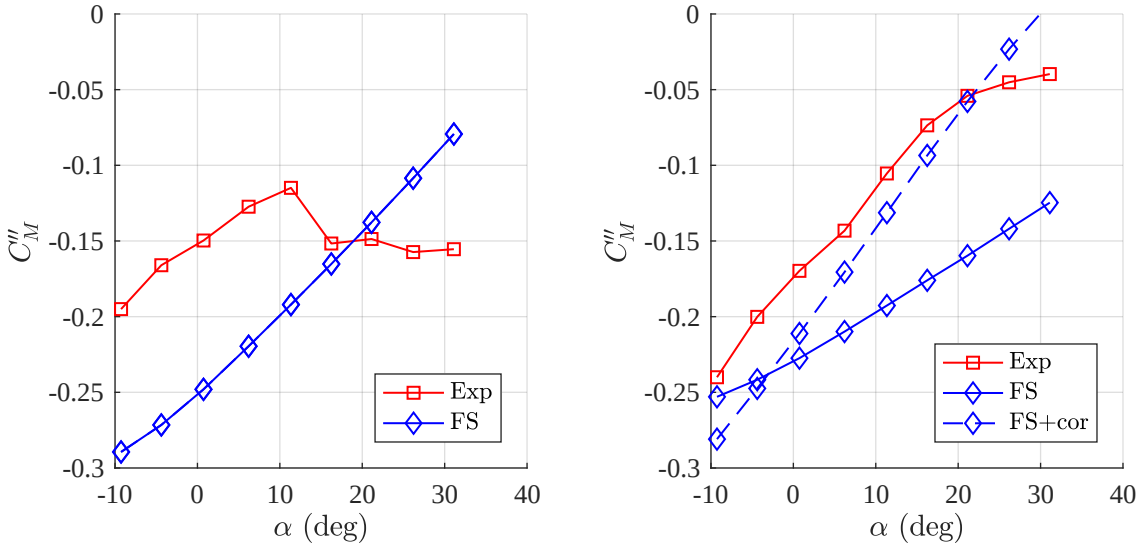

(a) $T''_c = 0$

(b) $T''_c = 0.50$

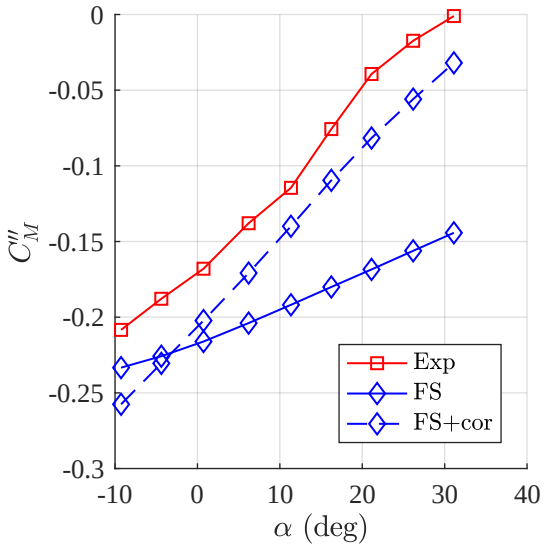

(c) $T''_c = 0.71$

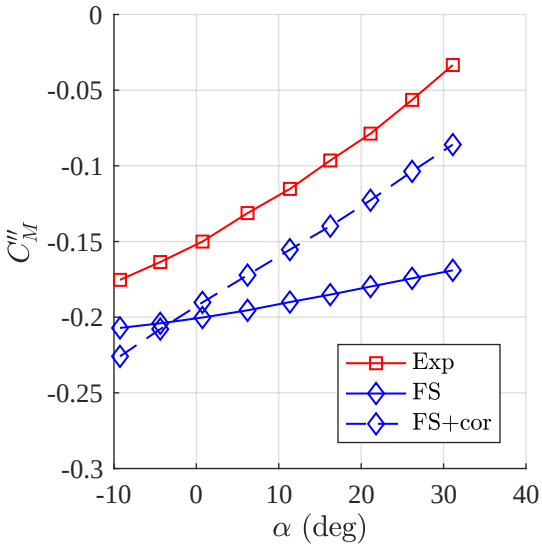

(d) $T''_c = 0.91$

Fig. 16 Comparison of experimental data and FlightStream predictions of slipstream-normalized pitching moment coefficient vs. angle of attack for varying slipstream-normalized thrust coefficients. 30% flap deflected 30°.

Acknowledgments

This work was funded under the Transformational Tools and Technologies Project of the Transformative Aeronautics Concepts Program.

References

[1] Ashby, D. L., "Potential Flow Theory and Operation Guide for the Panel Code PMARC 14," Tech. Rep. TM-1999-209582, National Aeronautics and Space Administration, 1999.

[2] Drela, M., and Youngren, H., "AVL," http://web.mit.edu/drela/Public/web/avl/, 2017. Accessed: 2018-11-29.

[3] Deperrois, A., "XFLR5," http://www.xflr5.com/xflr5.htm, 2018. Accessed: 2018-11-29.

[4] "Research in Flight," https://www.researchinflight.com/, 2018. Accessed: 2018-11-27.

[5] Ahuja, V., "Aerodynamic Loads Over Arbitrary Bodies by Method of Integrated Circulation," Ph.D. thesis, Auburn University, 2013.

[6] Ahuja, V., and Hartfield, R., "Aerodynamic Loads Over Arbitrary Bodies by Method of Integrated Circulation," *Journal of Aircraft*, 2016.

[7] Conway, J. T., "Analytical Solutions for the Actuator Disk with Variable Radial Distribution of Load," *Journal of Fluid Mechanics*, Vol. 297, 1995, pp. 327–355.

[8] Ahuja, V., and Hartfield, R., "Predicting the Aero Loads Behind a Propeller in the Presence of a Wing Using Flightstream," *15th AIAA Aviation Technology, Integration, and Operations Conference*, 2015.

[9] King, L., Ahuja, V., and Hartfield, R., "Aerodynamic Optimization of Integrated Wing-Engine Geometry Using an Unstructured Vorticity Solver," *33rd AIAA Applied Aerodynamics Conference*, 2015.

[10] Ahuja, V., Burkhalter, J. E., and Hartfield, R. J., "Optimizing Engine Placement on an Aircraft Wing using Bio-mimetic optimization and FlightStreamTM," *55th AIAA Aerospace Sciences Meeting*, 2017, p. 0235.

[11] Olson, E. D., and Albertson, C. W., "Aircraft High-Lift Aerodynamic Analysis Using a Surface-Vorticity Solver," *54th AIAA Aerospace Sciences Meeting*, 2016.

[12] Sandoz, B., Ahuja, V., and Hartfield, R. J., "Longitudinal Aerodynamic Characteristics of a V/STOL Tilt-wing Four-Propeller Transport Model using a Surface Vorticity Flow Solver," *2018 AIAA Aerospace Sciences Meeting*, 2018, p. 2070.

[13] Johnson, S., van Dommelen, D., Ahuja, V., and Hartfield, R. J., "Investigation of the Static Longitudinal Characteristics of a Full-Scale Light Single-Engine Airplane using a Surface Vorticity Solver," *2018 AIAA Aerospace Sciences Meeting*, 2018, p. 1259.

[14] Sargent, P. B., and Anemaat, W. A., "Benchmarking a Robust Panel Code for Ducted Fan VTOL Aircraft Design," *2018 Applied Aerodynamics Conference*, 2018, p. 4212.

[15] Anemaat, W. A., van Dommelen, D., Johnson, S., Sargent, P. B., and Liu, W., "Comparison of Aerodynamic Analysis Tools for Rotorcraft in Hover," *2018 AIAA Aerospace Sciences Meeting*, 2018, p. 2069.

[16] Borer, N. K., Patterson, M. D., Viken, J. K., Moore, M. D., Bevirt, J., Stoll, A. M., and Gibson, A. R., "Design and Performance of the NASA SCEPTOR Distributed Electric Propulsion Flight Demonstrator," *16th AIAA Aviation Technology, Integration, and Operations Conference*, 2016.

[17] Kuhn, R. E., and Draper, J. W., "An Investigation of a Wing-Propeller Configuration Employing Large-Chord Plain Flaps and Large-Diameter Propellers for Low-Speed Flight and Vertical Take-Off," Tech. Rep. TN 3307, National Advisory Committee for Aeronautics, 1954.

[18] Draper, J. W., and Kuhn, R. E., "Investigation of the Aerodynamic Characteristics of a Model Wing-Propeller Combination and of the Wing and Propeller Separately at Angles of Attack up to 90°," Tech. Rep. TN 3304, National Advisory Committee for Aeronautics, 1954.

[19] Kuhn, R. E., and Draper, J. W., "Investigation of the Aerodynamic Characteristics of a Model Wing-Propeller Combination and of the Wing and Propeller Separately at Angles of Attack up to 90 degrees," Tech. Rep. TR 1263, National Advisory Committee for Aeronautics, 1956.